AIMS Mathematics, 11(3): 8355–3181.
DOI: 10.3934/math.2026343
Received: 09 February 2026
Revised: 15 March 2026
Accepted: 24 March 2026
Published: 30 March 2026

http://www.aimspress.com/journal/Math

Research article

Modeling complex financial dynamics via Lie symmetry and chaos analysis of the generalized Black–Scholes equation

Khizar Farooq[1], Ali. H. Tedjani[2], Muhammad Amin S. Murad[3], Yakup Yildirim[4,5] and Taha Radwan[6,*]

[1] Centre for High Energy Physics, University of the Punjab, Quaid-e-Azam Campus, Lahore 54590, Pakistan

[2] Department of Mathematics and Statistics, College of Science, Imam Mohammad Ibn Saud Islamic University (IMSIU), Riyadh 11564, Saudi Arabia

[3] Department of Mathematics, College of Science, University of Duhok, Duhok 42001, Iraq

[4] Department of Computer Engineering, Biruni University, Istanbul–34010, Turkey

[5] Mathematics Research Center, Near East University, 99138 Nicosia, Cyprus

[6] Department of Management Information Systems, College of Business and Economics, Qassim University, Buraydah 51452, Saudi Arabia

* **Correspondence:** Email: t.radwan@qu.edu.sa.

Abstract: The classical Black–Scholes equation has a central role in the theory of option pricing; however, the classical form lacks sufficient power to model complex non-linear market effects, such as sudden asset price movements, volatility clustering, and instability. In this work, we consider a generalized nonlinear Black–Scholes equation aimed at providing a more faithful description of these types of complex behaviors. Initial analytical tractability is obtained with the application of Lie symmetry analysis, which leads to symmetry generators and similarity reductions that reduce the partial differential equation under consideration to lower-dimensional ordinary differential equations. The resulting reduced equation is solved analytically using the generalized Arnous (GA) method, resulting in a spectrum of exact solutions, bright and dark solitons, and exponential and trigonometric families of solutions. The dynamical characteristics of the reduced system are then examined using bifurcation analysis and chaos diagnostics. Numerical investigations involve phase portraits, Poincaré sections, return maps, Lyapunov exponents, and bifurcation diagrams, which reveal transitions to different regimes (periodic, quasi-periodic, and chaotic) under the influence of external perturbations. These results prove that the generalized model can have complex nonlinear dynamics and multistability, which can provide information about the irregular fluctuations of option prices in financial markets. The contribution of this work is the coherent combination of Lie symmetry reduction, the GA analytical framework, and nonlinear dynamical analysis of the generalized Black–Scholes equation, providing an

overall paradigm that could be used to explore complex financial dynamics.

Keywords: mathematical model; generalized Black–Scholes equation; Lie symmetry analysis; bifurcation analysis; generalized Arnous method; soliton solutions; chaotic behavior; multistability; chaotic attractor; Lyapunov exponent
Mathematics Subject Classification: 37K40, 39B62, 33B10, 26A48, 26A51

1. Introduction

The Black–Scholes equation (BSE) was introduced by Fischer Black and Myron Scholes in 1973 [1]. It is a fundamental model for pricing options and derivatives in financial markets [4]. It provides a mathematical framework that is used to estimate the fair value of European-style options by considering factors such as the underlying asset's price, the strike price, time to expiration, risk-free interest rates, and constant volatility. This model has had a great impact on finance, permitting investors and traders to assess the risk and make informed decisions about option contracts.

Formulation of the model

The importance of the BSE not only lies across asset management and arbitrage trading but also has a wide role in modern financial theory and practice [2,3]. This model won the Nobel Prize in Economic Sciences in 1997, highlighting its importance in financial markets. Although this model works under many assumptions, including efficient markets, volatility leads to notable criticism of its application in real-world problems when the market is complex and unpredictable.
The underlying asset price S(t) is defined as

$$dS = \mu S\,dt + \sigma\, S\; dW_t, \tag{1.1}$$

where μ denotes the expected return, σ shows the volatility, and W_t represents the Wiener process. For an option price, Itô's lemma gives

$$dQ = \left(\frac{\partial Q}{\partial t} + \mu S\frac{\partial Q}{\partial S} + \frac{1}{2}\sigma^2 S^2\frac{\partial^2 Q}{\partial S^2}\right)dt + \sigma S\frac{\partial Q}{\partial S}dW_t. \tag{1.2}$$

For risk-free portfolio construction, we use $\Pi = Q - \Delta S$ with $\Delta = \frac{\partial Q}{\partial S}$, which eliminates the stochastic component. Substituting Eqs (1.1) and (1.2), we have

$$d\Pi = \left(\frac{\partial Q}{\partial t} + \frac{1}{2}\sigma^2 S^2\frac{\partial^2 Q}{\partial S^2}\right)dt. \tag{1.3}$$

The portfolio is risk-free, so $d\Pi = r\Pi\,dt$. Equating (1.3) to $r(Q - \Delta S)dt$, we get BSE for the European option as follows:

$$\frac{\partial Q}{\partial t} + \frac{1}{2}\sigma^2 S^2\frac{\partial^2 Q}{\partial S^2} + rS\frac{\partial Q}{\partial S} - rQ = 0, \tag{1.4}$$

where $Q(S,t)$ is the option price, S is the underlying asset price, σ is volatility, r is the risk-free rate, and t is time. After the construction of this model, various generalizations were made.

The assumption of constant volatility in the BSE is not realistic. The Heston model [5] assumes that the volatility changes randomly with time, which leads to explaining the volatility seen in market data. The Heston model assumes the asset price S_t and its variance ν_t as,

$$\begin{cases} dS = \mu S\, dt + \sqrt{\nu_t} S\, dW_t^1, \\ d\nu_t = \kappa(\theta - \nu_t)dt + \xi \sqrt{\nu_t} dW_t^2, \end{cases} \tag{1.5}$$

where ν_t is instantaneous variance, κ is the mean reversion rate, θ is long-term variance, and ξ is the volatility of volatility. By using multi-dimensional Itô's lemma $Q(S, \nu, t)$, Eq (1.3) transforms into:

$$\frac{\partial Q}{\partial t} + \frac{1}{2}\, \nu\, S^2 \frac{\partial^2 Q}{\partial S^2} + \frac{1}{2}\xi^2\, \nu \frac{\partial^2 Q}{\partial \nu^2} + \rho\, \xi\, \nu\, S\, \frac{\partial^2 Q}{\partial S\, \partial \nu} + r\, S\, \frac{\partial Q}{\partial S} + \kappa(\theta - \nu)\frac{\partial Q}{\partial \nu} - rQ = 0. \tag{1.6}$$

The Heston model is used to price options on stocks and other assets because it better captures the real market behavior, including how volatility changes over time.

Market returns sometimes change suddenly, showing Brownian motions that cannot be captured. To address this difficulty, Merton's jump-diffusion model [6] incorporates bumps, which enhance the accuracy of option pricing. In this model, the asset price S_t is modified as follows:

$$dS_t = \mu S_t\, dt + \sigma S_t\, dW_t + S_t(e^J - 1)\, dN_t, \tag{1.7}$$

where N_t is a Poisson process with intensity λ, and J is the log-normal jump size. By using Eq (1.7), Eq (1.3) transforms into

$$\frac{\partial Q}{\partial t} + \frac{1}{2}\sigma^2 S^2 \frac{\partial^2 Q}{\partial S^2} + (r - \lambda \bar{J})S \frac{\partial Q}{\partial S} - (r + \lambda)Q + \lambda \mathbb{E}[Q(S(1 + J), t)] = 0. \tag{1.8}$$

This model is useful for assets that experience sudden jumps in price, like stocks during economic news or earnings reports, making hedging more effective against the jump risk.

Interests affect the stock price, but the Black–Scholes model does not account for this. Therefore, it needs adjustments to correctly price options on the stocks that pay interest [7].

If the stock pays a continuous interest at a rate of M, then the price changes as follows:

$$dS = (\mu - M)S\, dt + \sigma S\, dW. \tag{1.9}$$

By using Eq (1.9), Eq (1.3) transforms into

$$\frac{\partial Q}{\partial t} + (r - M)S \frac{\partial Q}{\partial S} + \frac{1}{2}\sigma^2 S^2 \frac{\partial^2 Q}{\partial S^2} - rQ = 0. \tag{1.10}$$

This adjustment is significant for accurately pricing options on interest-paying stocks and making sure that the model reflects the return investors receive.

Local volatility models [8] surpass the assumption of constant volatility. Instead of treating volatility as a constant function of asset price and time, $\sigma = \sigma(S, t)$ helps to capture the full suggested volatility surface.

$$\sigma^2(K, T) = \frac{1}{K^2}\left(\frac{\partial^2 Q}{\partial K^2}\right) \Big/ \left(\frac{\partial Q}{\partial T} + rK\frac{\partial Q}{\partial K}\right), \tag{1.11}$$

where $Q = Q(K, T)$ is the call price and K is a strike and T is maturity. Local volatility models are mostly used to price exotic options and show how volatility changes in the market.

Market conditions change over time, so fixed interest rates are not realistic. If these values vary with time, then it will make our model more realistic. If the risk-free rate $r(t)$ and volatility $\sigma(t)$ varies with time, the BSE will become [9]

$$\frac{\partial Q}{\partial t} + r(t)S\frac{\partial Q}{\partial S} + \frac{1}{2}\sigma^2(t)S^2\frac{\partial^2 Q}{\partial S^2} - r(t)Q = 0. \tag{1.12}$$

This model is significant when interest rates and economic policies change a lot over time.
The generalization of the BSE, which we discuss in this article, is [10]

$$Q_t + \frac{1}{2}E^2x^2\,Q_{xx} + F\,x\,Q_x - G\,Q + H\,Q^3 = 0. \tag{1.13}$$

Here, $Q(x, t)$ is the interest function which represents the option price, $(\frac{1}{2}E^2x^2Q_{xx})$ represents the volatility term modeling the diffusion of the option value concerning the underlying asset price, FxQ_x is related to the underlying asset's growth rate, (GQ) defines the interest rate, and (HQ^3) captures market effects such as feedback, transaction costs, and other frictions that cannot be explained by the standard linear model. This nonlinear extension provides a more accurate framework for capturing abrupt price changes and irregular volatility in the real market. More broadly, the generalized equation has a structural resemblance to nonlinear wave equations in physics, which show dispersion, dissipation, and nonlinearity wave behaviors. This similarity motivates the use of tools such as Lie symmetries, soliton theory, and chaos analysis to study option pricing in complex market settings.

Literature review

The binomial tree method was first constructed by Cros et al. [11] for the BSE. To find the option price at every node of the tree, Hull [12] introduced the trinomial tree method. Courtadon [13] applied the finite differential approach to find the variance in the generalized jump model of the BSE [14]. Log-transformation was applied to the BSE by Schwartz [14] before using the standard finite difference method to calculate the option price. The challenge of replacing European options by using the static portfolio of cash and underlying assets was addressed by Bossu [15]. The modified homotopy perturbation method, along with the Sumudu transformation, was applied to the fractional BSE by Ouafoudi [16]. Using the Mellin transformation to evaluate Eq (1.7) to incorporate the modified log-payoff function under geometric Brownian motion was studied by Fadugba [17]. The partial series Taylor expansion method was applied to the BSE for the log-payoff function by Sobamowo [18]. Double barrier options using the time-fractional BSE was explored by Tour [19]. A semi-analytical approach was applied to the BSE to find the solution for pricing European call options by Durojaye [20]. Two semi-analytical methods were applied to the BSE by Fadugba [21]. The fractional complex modified differential transform method was applied to the BSE with non-integer order by Edeki [22]. Homotopy analysis via the Shehu transform method was applied to the fractional BSE by Vijayan [23]. The neural network model was applied to the BSE to find the option price in a European call by de Souza Santos [24]. A numerical approach was applied to the BSE with static volatility by Eric Ngondiep [25]. The conformable Shehu homotopy analysis method was applied to the two-dimensional BSE by Chandrasekaran [26]. Zavyalova and Timofeeva [27] investigated

the dynamics of the abrupt price changes in the BSE model by applying a stability analysis under spasmodic volatility. Afiatdoust et al. [28] applied generalized shifted Chebyshev polynomials to the time-fractional BSE by converting it into an algebraic system. Ait Brahim et al. [29] proposed a new generalized fractional BSE using novel conformable derivatives for option pricing. Sukwong et al. [30] investigated the time-fractional multi–asset Black–Scholes option pricing model by using the generalized Laplace residual power series method. A generalized conformable Black–Scholes model was formulated by Morales-Bañuelos et al. [31] through the application of seven conformable derivatives, yielding improved empirical performance over classical models. Furthermore, Vijayan et al. [32] extended the literature by addressing the conformable-fractional BSE with three analytical schemes: Variational iteration, reduced differential transform, and homotopy analysis methods in the conformable sense.

Research aim and objectives

A careful examination of the literature reveals that no work addresses the Lie point symmetry of Eq (1.13) together with its dynamical properties, such as its bifurcation analysis, chaotic behavior, multistability, Lyapunov exponent, Chaotic attractor, return map, and bifurcation diagram. Furthermore, no attempt has been made to derive solitary wave solutions using the generalized Arnous (GA) method. In the present study, we fill this gap by investigating Lie point symmetry, constructing solitary waves using the GA method, and performing a detailed dynamical analysis of Eq (1.13).

Contribution and originality

The novelty of the present investigation lies in the fact that a cohesive analytical and dynamical framework for the generalized nonlinear BSE is formulated. This work applies Lie symmetry analysis to the identification of symmetry generators and implementation of similarity reductions to transform the governing partial differential equation (PDE) into a system of reduced ordinary differential equations (ODEs). The resulting nonlinear ordinary differential equation is analytically solved using the Generalized Arnous method to give several classes of exact solutions, namely bright soliton, dark soliton, trigonometric, and exponential-type solutions. Furthermore, the non-linear dynamical properties of the reduced system are investigated by phase portrait construction, equilibrium point analysis, and bifurcation studies. The model is then extended by adding periodic perturbations to it in order to study the dynamics of chaos using the Lyapunov exponents, bifurcation diagrams, return maps, and chaotic attractors. To our knowledge, the combination of Lie symmetry reduction, analytical soliton construction with the GA scheme, and detailed chaos analysis for the generalized BSE has not been reported before.

Summarization

The whole article is summarized as follows: In Section 1, we introduce our model, and Table 1 shows the Nomenclature of parameters and variables used in this study. In Section 2, an infinitesimal transformation is applied to the system to construct the Lie point generators. Section 3 presents the symmetry reduction with the help of generators. In Section 4, we apply the GA method to construct the solitary solutions, and in Table 2, a comparison with the literature is discussed. In Section 5, we discuss

the bifurcation analysis with the aid of equilibrium points. Section 6 represents the chaotic behavior of our system along with the related multistability, Lyapunov exponent, chaotic attractor, return map, and bifurcation diagram. Section 9 concludes our manuscript.

Table 1. Nomenclature of parameters and variables used in this study.

Symbol	Description/physical meaning
S	Underlying asset price
t	Time variable
$Q(S,t)$	Option value function in the generalized Black–Scholes framework
r	Risk-free interest rate
σ	Volatility of the underlying asset
μ	Drift or expected return rate of the asset
H	Coefficient of the cubic nonlinear term in the generalized BSE
η	Coefficient of the quintic nonlinear term
λ	Bifurcation or control parameter in nonlinear dynamics
γ	Model parameter governing feedback or gain
α	Scaling constant used in Lie symmetry transformations
β	Shape parameter controlling the solution's width or scaling
ϵ	Perturbation or diffusion coefficient in the transformed equation
ξ	Traveling-wave or similarity transformation variable
ω	Frequency or wave-number parameter
$\Phi(S,t)$	Phase function appearing in the analytical solution ansatz
$R(\xi)$	Amplitude function obtained after similarity reduction
ρ	Density-like function used in probabilistic representation
$K(\xi)$	Generalized exponential rational expression used for constructing analytical solutions
a_i, b_i	Integration constants or balance coefficients appearing in the analytical ansatz
D_t	Temporal differential operator
D_S	Spatial (asset price) differential operator
Ψ	Perturbation frequency used in chaotic analysis
P	Parameter space considered in bifurcation and chaos analysis

2. Lie symmetry assessment

In recent years, Lie symmetry analysis [33] of several extensions of the BSE has become common. In particular, the research group of Yu and Feng has contributed extensively to this area using

symmetry analysis to fractional and generalized Black-Scholes models. Their studies obtained Lie point symmetries, invariant solutions, and conservation laws for various forms of the BSE, and thus gave a better insight into the analytical structure and solution behavior of financial PDE models. These works show the success of Lie symmetry techniques for analyzing the nonlinear and fractional option pricing equations [34].

Assume a Lie group transformation with a parameter (η) to construct the generators for Eq (1.13) as [35] follows:

$$\begin{aligned} \mathcal{T}^* &= \mathcal{T} + \eta\,\lambda(\mathcal{T},\mathcal{X},\mathcal{Q}) + O(\eta^2), \\ \mathcal{X}^* &= \mathcal{X} + \eta\,\delta(\mathcal{T},\mathcal{X},\mathcal{Q}) + O(\eta^2), \\ \mathcal{Q}^* &= \mathcal{Q} + \eta\,\epsilon(\mathcal{T},\mathcal{X},\mathcal{Q}) + O(\eta^2), \end{aligned} \tag{2.1}$$

where $\eta < 1$, and λ, δ, and ϵ are the infinitesimal unknown constants depending on $\mathcal{X}$, $\mathcal{T}$, and $\mathcal{Q}$ in Eq (2.1). The generators can be found using the corresponding vector field as:

$$\mathcal{L}^* = \lambda(\mathcal{T},\mathcal{X},\mathcal{Q})\,\frac{\partial}{\partial\mathcal{T}} + \delta(\mathcal{T},\mathcal{X},\mathcal{Q})\,\frac{\partial}{\partial\mathcal{X}} + \epsilon(\mathcal{T},\mathcal{X},\mathcal{Q})\,\frac{\partial}{\partial\mathcal{Q}}. \tag{2.2}$$

The corresponding invariant condition for Eq (1.13) with $\mathcal{L}^*$ is given as follows:

$$\mathcal{L}^{*[2]}\left[\mathcal{Q}_{\mathcal{T}} + \frac{1}{2}E^2\mathcal{X}^2\,\mathcal{Q}_{\mathcal{X}\mathcal{X}} + F\,\mathcal{X}\,\mathcal{Q}_{\mathcal{X}} - G\,\mathcal{Q} + H\,\mathcal{Q}^3\right]_{|Eq.(1.13)=0} = 0. \tag{2.3}$$

Inevitably, the second prolongation formula for Eq (1.13) is

$$\mathcal{L}^{*[2]} = \mathcal{L}^* + \epsilon^{\mathcal{X}}\frac{\partial}{\partial\mathcal{Q}_{\mathcal{X}}} + \epsilon^{\mathcal{T}}\frac{\partial}{\partial\mathcal{Q}_{\mathcal{T}}} + \epsilon^{\mathcal{X}\mathcal{X}}\frac{\partial}{\partial\mathcal{Q}_{\mathcal{X}\mathcal{X}}}. \tag{2.4}$$

$\epsilon^{\mathcal{X}}, \epsilon^{\mathcal{T}}, \epsilon^{\mathcal{X}\mathcal{X}}$ are the extended infinitesimals represented as follows:

$$\begin{aligned} \epsilon^{\mathcal{T}} &= \Theta_{\mathcal{T}}(\epsilon) - \mathcal{Q}_{\mathcal{T}}\Theta_{\mathcal{T}}(\lambda) - \mathcal{Q}_{\mathcal{X}}\Theta_{\mathcal{T}}(\delta), \\ \epsilon^{\mathcal{X}} &= \Theta_{\mathcal{X}}(\epsilon) - \mathcal{Q}_{\mathcal{T}}\Theta_{\mathcal{X}}(\lambda) - \mathcal{Q}_{\mathcal{X}}\Theta_{\mathcal{X}}(\delta), \\ \epsilon^{\mathcal{X}\mathcal{X}} &= \Theta_{\mathcal{X}}(\epsilon^{\mathcal{X}}) - \mathcal{Q}_{\mathcal{T}\mathcal{X}}\Theta_{\mathcal{X}}(\lambda) - \mathcal{Q}_{\mathcal{X}\mathcal{X}}\Theta_{\mathcal{X}}(\delta). \end{aligned} \tag{2.5}$$

The condition $\mathcal{L}^{*[2]}$(Eq (1.13)) with Eq (1.13) = 0 gives the invariance equation

$$\epsilon_{\mathcal{T}} + \frac{1}{2}E^2\mathcal{X}^2\,\epsilon_{\mathcal{X}\mathcal{X}} + F\,\mathcal{X}\,\epsilon_{\mathcal{X}} - G\,\epsilon + H\,\epsilon^3 = 0. \tag{2.6}$$

Substituting $\epsilon^{\mathcal{X}}, \epsilon^{\mathcal{T}}$ and $\epsilon^{\mathcal{X}\mathcal{X}}$ into the given equation, and setting the coefficient of different derivative terms to zero, we obtain a system of PDEs. Solving this system yields the following infinitesimals:

$$\eta = c_2\mathcal{X}, \quad \delta = c_1, \quad \epsilon = 0, \tag{2.7}$$

where c_1 and c_2, are the arbitrary constants. The vector fields are defined in the theorem below, which governs the Lie algebra of infinitesimal symmetries in Eq (2.7).

Theorem 1. Equation (2.7) exhibits a two-dimensional Lie algebra explained by the two generators as follows:

$$\mathcal{L}_1^* = \frac{\partial}{\partial\mathcal{T}}, \quad \mathcal{L}_2^* = \mathcal{X}\frac{\partial}{\partial\mathcal{X}}. \tag{2.8}$$

We need to solve three ordinary differential equations when $\mathcal{K}_i$ is covered by $\mathcal{L}_i^*$ for (i = 1,2) to analyze the symmetry group.

$$\begin{aligned}
\frac{d(\tilde{\mathcal{T}})}{d\epsilon} &= \lambda(\tilde{\mathcal{T}}, \tilde{\mathcal{X}}, \tilde{\mathcal{Q}}), \quad with \quad \tilde{\mathcal{T}}|_{\epsilon=0} = \mathcal{T}, \\
\frac{d(\tilde{\mathcal{X}})}{d\epsilon} &= \delta(\tilde{\mathcal{T}}, \tilde{\mathcal{X}}, \tilde{\mathcal{Q}}), \quad with \quad \tilde{\mathcal{X}}|_{\epsilon=0} = \mathcal{X}, \\
\frac{d(\tilde{\mathcal{Q}})}{d\epsilon} &= \lambda(\tilde{\mathcal{T}}, \tilde{\mathcal{X}}, \tilde{\mathcal{Q}}), \quad with \quad \tilde{\mathcal{Q}}|_{\epsilon=0} = \mathcal{Q},
\end{aligned} \tag{2.9}$$

where ϵ is the infinitesimal parameter. The following symmetry group $\mathcal{K}_i$ covered by $\mathcal{L}_i^*$ can be constructed with help of the generators λ, δ, and ϵ.

$$\begin{aligned}
\mathcal{K}_1^{*\dagger} &: (\mathcal{T}, \mathcal{X}, \mathcal{Q}) \to (\mathcal{T} + \epsilon, \mathcal{X}, \mathcal{Q}), \\
\mathcal{K}_2^{*\dagger} &: (\mathcal{T}, \mathcal{X}, \mathcal{Q}) \to (\mathcal{T}, e^{\epsilon}\mathcal{X}, \mathcal{Q}), \\
\mathcal{K}_3^{*\dagger} &: (\mathcal{T}, \mathcal{X}, \mathcal{Q}) \to (\mathcal{T}, \mathcal{X}, \mathcal{Q}).
\end{aligned} \tag{2.10}$$

Here, $\mathcal{K}_i^{*\dagger}$ is temporal, and $\mathcal{K}_2^{*\dagger}$ and $\mathcal{K}_3^{*\dagger}$ exhibit space invariance.

Theorem 2. The new solution can be obtained by applying $\mathcal{K}_i^{*\dagger}$ $1 \leq i \leq 2$. If $\mathcal{Q}(\mathcal{X}, \mathcal{T})$ is taken as the solution of Eq (1.13), then by using $\mathcal{K}_i^{*\dagger}$ for $1 \leq i \leq 2$, the new solution $\mathcal{Q}_i$ for $1 \leq i \leq 2$ is obtained as follows:

$$\begin{aligned}
\mathcal{K}_1^{*\dagger}(\epsilon)\, \mathcal{Q}_1(\mathcal{T}, \mathcal{X}) &= \tilde{\mathcal{Q}}_1(\mathcal{T} - \epsilon, \mathcal{X})\mathcal{K}_1^{*\dagger}(\epsilon), \\
\mathcal{K}_2^{*\dagger}(\epsilon)\, \mathcal{Q}_2(\mathcal{T}, \mathcal{X}) &= \tilde{\mathcal{Q}}_2(\mathcal{T}, \mathcal{X}e^{\epsilon})\mathcal{K}_2^{*\dagger}(\epsilon), \\
\mathcal{K}_3^{*\dagger}(\epsilon)\, \mathcal{Q}_3(\mathcal{T}, \mathcal{X}) &= \tilde{\mathcal{Q}}_3(\mathcal{T}, \mathcal{X})\mathcal{K}_3^{*\dagger}(\epsilon).
\end{aligned} \tag{2.11}$$

By applying the Lie bracket, defined as $[\mathcal{L}_m^*\mathcal{L}_n^*] = \mathcal{L}_m^*\mathcal{L}_n^* - \mathcal{L}_n^*\mathcal{L}^*{}_m$, the commutators can be mathematically stated as follows:

$$[\mathcal{L}_m^*, \mathcal{L}_n^*] = [\mathcal{L}_n^*, \mathcal{L}_m^*] = 0, \quad m, n = 1, 2. \tag{2.12}$$

In the subsequent stage of our inquiry, we seek to ascertain the adjoint illustrations of the vector fields. To support this investigation, we use the following Lie as the basis for our inquiry:

$$\mathrm{Ad}_{\exp(\epsilon\mathcal{L}^*{}_m)}(\mathcal{L}^*{}_n) = \mathcal{L}^*{}_n - \epsilon[\mathcal{L}^*{}_m, \mathcal{L}^*{}_n] + \frac{\epsilon^2}{2!}[\mathcal{L}^*{}_m, [\mathcal{L}^*{}_m, \mathcal{L}^*{}_n]] - \cdots, \quad \text{for } \epsilon \in \mathbb{R}, \tag{2.13}$$

which results in

$$\begin{cases}
\mathrm{Ad}_{\exp(\epsilon\mathcal{L}^*{}_m)}(\mathcal{L}^*{}_n) = \mathcal{L}^*{}_m + O(\epsilon^2), & m = m, \\
\mathrm{Ad}_{\exp(\epsilon\mathcal{L}^*{}_m)}(\mathcal{L}^*{}_n) = \mathcal{L}^*{}_n + O(\epsilon^2), & m \neq n.
\end{cases} \tag{2.14}$$

The optimal systems can be inferred from the adjoint depictions Eq (2.14) as follows, with $\epsilon << 1$ representing a minor group parameter. An infinite array of symmetries is present for Eq (1.13).

Theorem 3. Let $\mathcal{P}_2^*$ be the Lie algebra of Eq (1.13) as defined in Eq (2.3). This set of generators offers a perfect framework of one-dimensional subalgebras:

$$\begin{aligned}
\mathcal{P}_1^* &= \langle \mathcal{L}_1^* \rangle, \\
\mathcal{P}_{1\alpha}^* &= \langle \mathcal{L}_2^* \rangle, \\
\mathcal{P}_2^* &= \langle \mathcal{L}_1^* + \eta\mathcal{L}_2^* \rangle, \quad \eta \neq 0.
\end{aligned} \tag{2.15}$$

Proof. Let $\mathcal{L}^*$ be an arbitrary element such that $\mathcal{L}^* \in \mathcal{P}_2^*$. We express it as:

$$\mathcal{L}^* = S_1\mathcal{L}_1^* + S_2\mathcal{L}_2^*. \tag{2.16}$$

Case 1. $S_2 = 0$ and $S_1 = 1$. Then

$$\mathcal{L}^* = \mathcal{L}_1^*, \tag{2.17}$$

and thus

$$\mathcal{P}_1^* = \langle \mathcal{L}_1^{*\dagger} \rangle. \tag{2.18}$$

Case 2. $S_1 = 0$ and $S_2 = 1$. Then

$$\mathcal{L}^* = \mathcal{L}_2^*, \tag{2.19}$$

and thus

$$\mathcal{P}_{1\alpha}^* = \langle \mathcal{L}_2^* \rangle. \tag{2.20}$$

Case 3. $S_1 = 1$ and $S_2 \neq 0$. Then

$$\mathcal{L}^* = \mathcal{L}_1^* + S_2\mathcal{L}_2^*. \tag{2.21}$$

Taking $S_2 = \eta$, we have

$$\mathcal{P}_2^* = \langle \mathcal{L}_1^* + \eta\mathcal{L}_2^* \rangle. \tag{2.22}$$

3. Symmetry reduction techniques and explicit solution

This section applies symmetry reduction methods for reducing the governing PDE to individual symmetries and combinations of symmetries to ODEs. Moreover, a number of explicit solutions are obtained after reducing the equations.

3.1. Reduction through translation invariance: $\mathcal{L}_1^* = \frac{\partial}{\partial \mathcal{T}}$

The characteristic equation of the operator, which is the case of the operator of L_1^*, is as follows:

$$\frac{dx}{0} = \frac{dt}{1} = \frac{d\mathcal{Q}}{0}. \tag{3.1}$$

The solution of the characteristic equation (3.1) gives the following results:

$$x = \mathcal{M}, \quad \mathcal{Q} = \mathcal{N}, \quad \mathcal{N} = \mathcal{P}(\mathcal{M}), \quad \mathcal{Q} = \mathcal{P}(\mathcal{M}), \tag{3.2}$$

where $\mathcal{M}$ and $\mathcal{N}$ are arbitrarily constant. Hence the solution can be expressed in function form as $\mathcal{N} = \mathcal{P}(\mathcal{M})$; consequently $\mathcal{Q} = \mathcal{P}(\mathcal{M})$.

By substituting this function given in Eq (3.2) into Eq (1.13), the generalized BSE is reduced to the following form:

$$\frac{1}{2}E^2x^2\,\mathcal{P}(\mathcal{M})'' + F\,x\,\mathcal{P}(\mathcal{M})' - G\,\mathcal{P}(\mathcal{M}) + H\,\mathcal{P}(\mathcal{M})^3 = 0. \tag{3.3}$$

3.2. Reduction through translation invariance: $\mathcal{L}_2^* = x\frac{\partial}{\partial \mathcal{T}}$

The characteristic equation of the operator, which is the case of the operator of L_2^*, is as follows:

$$\frac{dx}{x} = \frac{dt}{0} = \frac{d\mathcal{Q}}{0}. \tag{3.4}$$

The solution of the characteristic equation (3.4) gives the following results:

$$t = \mathcal{M}, \quad \mathcal{Q} = \mathcal{N}, \quad \mathcal{N} = \mathcal{P}(\mathcal{M}), \quad \mathcal{Q} = \mathcal{P}(\mathcal{M}), \tag{3.5}$$

where $\mathcal{M}$ and $\mathcal{N}$ are arbitrarily constant. Hence the solution can be expressed in function form as $\mathcal{N} = \mathcal{P}(\mathcal{M})$; and consequently, $\mathcal{Q} = \mathcal{P}(\mathcal{M})$.

By substituting this function given in Eq (3.5) into Eq (1.13), the generalized BSE is reduced to the following form:

$$\mathcal{P}(\mathcal{M})' - G\,\mathcal{P}(\mathcal{M}) + H\,\mathcal{P}(\mathcal{M})^3 = 0. \tag{3.6}$$

3.3. Reduction through translation invariance: $\beta\mathcal{L}_1^* + \Omega\mathcal{L}_2^*$

The characteristic equation of the operator, which is the case of the operator of $\beta L_1^* + \Omega L_2^*$, is as follows:

$$\frac{dx}{\Omega x} = \frac{dt}{\beta} = \frac{d\mathcal{Q}}{0}. \tag{3.7}$$

The solution of the characteristic equation (3.7) gives the following results:

$$\xi = \beta(\ln x) - \Omega t, \quad \mathcal{Q} = \mathcal{N}, \quad \mathcal{N} = \Re(\xi), \quad \mathcal{Q} = \Re(\xi), \tag{3.8}$$

where $\mathcal{M}$ and $\mathcal{N}$ are arbitrarily constant. Hence the solution can be expressed in function form as $\mathcal{N} = \mathcal{R}(\xi)$; consequently, $\mathcal{Q} = \mathcal{R}(\xi)$.

By substituting this function given in Eq (3.2) into Eq (1.13), the generalized BSE is reduced to the following form:

$$\frac{1}{2}E^2\beta^2\,\Re'' + \frac{1}{2}((E^2 + 2F)\beta - 2\omega)\,\Re' - G\,\Re + H\,\Re^3 = 0. \tag{3.9}$$

4. The GA method

The fundamental procedure for the GA method is outlined as follows.

Step 1. According to the GA method, the solution of Eq (3.9) can be expressed in the following form:

$$\Re(\xi) = A_0 + \sum_{i=1}^{N} \frac{A_i + B_i\mathcal{F}'(\xi)^i}{\mathcal{F}(\xi)^i}, \tag{4.1}$$

where A_0, A_i, B_i (for i = 1, 2, . . . , N) are real parameters satisfying the condition $A_N^2 + B_N^2 \neq 0$, and the function $\mathcal{F}(\xi)$ satisfies the following auxiliary equation:

$$[\mathcal{F}'(\xi)]^2 = [\mathcal{F}(\xi)^2 - \lambda]\ln[K], \tag{4.2}$$

along with

$$\mathcal{F}^{(n)}(\xi) = \begin{cases} \mathcal{F}(\xi)\ln(K)^n, & \text{if } n \text{ is even,} \\ \mathcal{F}'(\xi)\ln(K)^{n-1}, & \text{if } n \text{ is odd.} \end{cases} \tag{4.3}$$

In the above mentioned equation $n \geq 2$, and $0 < K \neq 1$. Equation (4.2) can be expressed in the following form:

$$\mathcal{F}(\xi) = M\ln(K)K^{\xi} + \frac{\lambda}{4M\ln}(K)K^{\xi}. \tag{4.4}$$

Here λ, M, and K are real constants.

Step 2. By balancing the non-linear term with the highest-order derivative in Eq (3.9), the positive integer N in Eq (4.1) can be as shown in [36].

Step 3. By substituting Eqs (4.1)–(4.3) in Eq (3.9) and by using the condition $Q^i(\xi) \neq 0$, the resulting equation becomes a polynomial in $\frac{1}{\mathcal{F}(\xi)}\left(\frac{\mathcal{F}'(\xi)}{\mathcal{F}(\xi)}\right)$. By equating the coefficients of the term with the identical power to zero, a system of non-linear algebraic equations is obtained. Solving this system, together with Eq (4.1) and Eq (3.8), yields the solutions of Eq (1.13).

4.1. Solutions by GA method

To derive the exact solution of Eq (3.9), the positive integer N is determined to be $N = 1$. Inserting this value into Eq (4.1) transforms the equation accordingly [40]:

$$\Re(\xi) = A_0 + \frac{A_1}{\mathcal{F}(\xi)} + \frac{B_1\mathcal{F}'(\xi)}{\mathcal{F}(\xi)}. \tag{4.5}$$

Next, Eq (4.3) is substituted into Eq (3.9) together with Eqs (3.8) and (4.2). This substitution produces a polynomial in terms of $\frac{1}{\mathcal{F}(\xi)}\left(\frac{\mathcal{F}'(\xi)}{\mathcal{F}(\xi)}\right)$. By collecting the coefficients of like powers and equating them to zero, a system of algebraic equations is obtained. Solving this system yields the value of the unknown constants.

Set 1.

$$A_0 = 0,\ \ A_1 = -\frac{\sqrt{2}\,\sqrt{G}\,\sqrt{\lambda}}{\sqrt{H}},\ \ B_1 = 0,\ \ F = \frac{1}{2}L\left(\frac{\sqrt{2}\omega\log(K)}{\sqrt{G}} - L\right),\ \ \beta = \frac{\sqrt{2}\,\sqrt{G}}{L\log(K)}. \tag{4.6}$$

By substituting Set 1 into Eq (4.5), the following exact solution is obtained:

$$Q_1(t,x) = -\frac{4\sqrt{2}\,\sqrt{G}\,\sqrt{\lambda}M\log(K)x^{\frac{\sqrt{2}\sqrt{G}}{L}}K^{t\Omega}}{\sqrt{H}\left(4M^2\log^2(K)x^{\frac{2\sqrt{2}\sqrt{G}}{L}} + \lambda K^{2t\Omega}\right)}. \tag{4.7}$$

When $K = e$ and $\lambda = 4M^2$ are selected, then Eq (4.7) takes the following form:

$$Q_2(t,x) = -\frac{\sqrt{2}\,\sqrt{G}M\operatorname{sech}\left(t\Omega - \frac{\sqrt{2}\,\sqrt{G}\log(x)}{L}\right)}{\sqrt{H}\,\sqrt{M^2}}. \tag{4.8}$$

Graphical visualization of the derived solution of Eq (4.8) that gives bright solitons is represented in Figure 1.

When $K = e$ and $\lambda = -4M^2$ are selected, then Eq (4.7) takes the following form:

$$Q_3(t,x) = \frac{\sqrt{2}\sqrt{G}\sqrt{-M^2}\operatorname{csch}\left(t\Omega - \frac{\sqrt{2}\sqrt{G}\log(x)}{L}\right)}{\sqrt{H}M}. \tag{4.9}$$

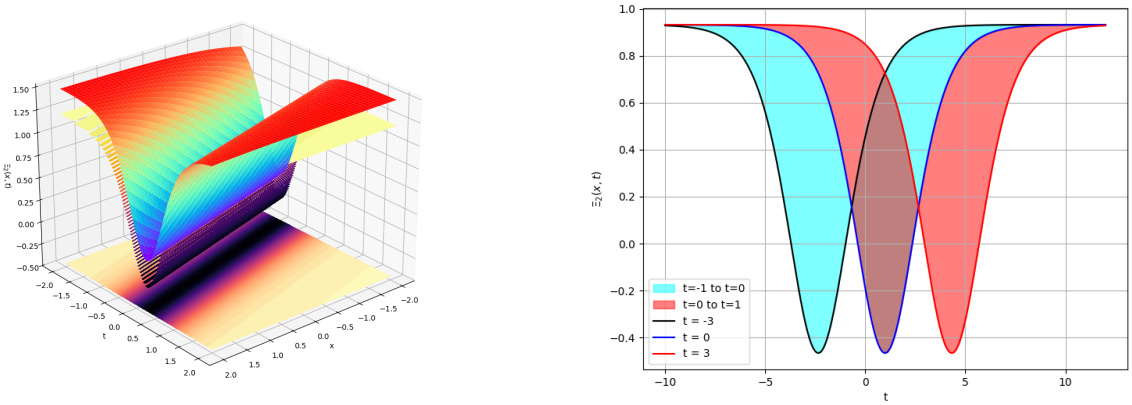

(a) 3D surface

(b) 2D surface

Figure 1. Graphical visualization of the derived solution of Eq (4.8) that gives bright solitons: (a) Three-dimensional (3D) surface and (b) two-dimensional (2D) surface of $Q_2(x,t) : G = 4, \quad M = 1, \quad \Omega = 1, \quad H = 2, \quad \lambda = -1, \quad E = 1$, and $K = 1.8$.

Set 2.

$$A_0 = 0, \quad A_1 = -\frac{\sqrt{2}\sqrt{G}\sqrt{\lambda}}{\sqrt{H}}, \quad B_1 = 0, \quad L = -\frac{\sqrt{2}\sqrt{G}}{\beta\log(K)}, \quad F = \frac{\beta\omega - \frac{G}{\log^2(K)}}{\beta^2}. \tag{4.10}$$

By substituting Set 2 into Eq (4.3), the following exact solution is obtained:

$$Q_4(t,x) = -\frac{4\sqrt{2}\sqrt{G}\sqrt{\lambda}M\log(K)K^{t\Omega+\beta\log(x)}}{\sqrt{H}\left(4M^2\log^2(K)K^{2\beta\log(x)} + \lambda K^{2t\Omega}\right)}. \tag{4.11}$$

Graphical visualization of the derived solution of Eq (4.11) that gives dark solitons is represented in Figure 2.

When $K = e$ and $\lambda = 4M^2$ are selected, then Eq (4.11) takes the following form:

$$Q_5(t,x) = -\frac{\sqrt{2}\sqrt{G}M\operatorname{sech}\left(t\Omega - \frac{\sqrt{2}\sqrt{G}\log(x)}{L}\right)}{\sqrt{H}\sqrt{M^2}}. \tag{4.12}$$

When $K = e$ and $\lambda = -4M^2$ are selected, then Eq (4.11) takes the following form:

$$Q_6(t,x) = \frac{\sqrt{2}\sqrt{G}\sqrt{-M^2}\operatorname{csch}\left(t\Omega - \frac{\sqrt{2}\sqrt{G}\log(x)}{L}\right)}{\sqrt{H}M}. \tag{4.13}$$

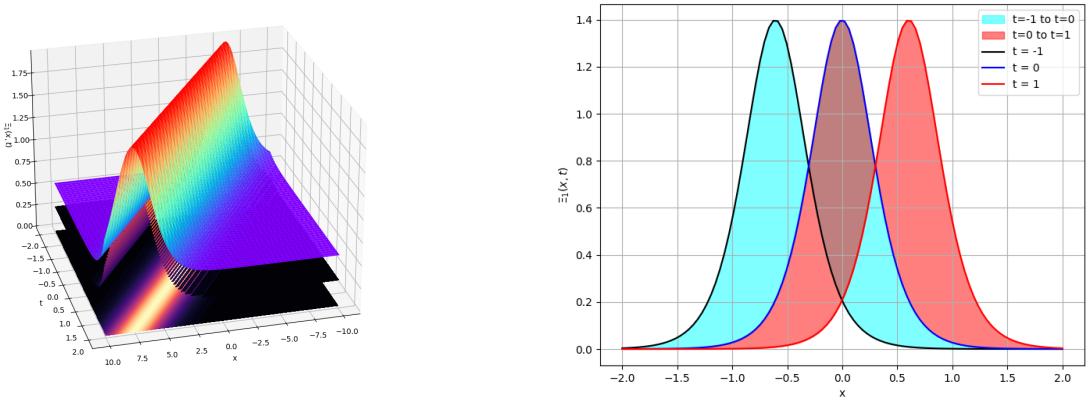

(a) 3D surface

(b) 2D surface

Figure 2. Graphical visualization of the derived solution of Eq (4.11) that gives dark solitons: (a) 3D surface and (b) 2D surface of $Q_4(x,t) : G = 4, \quad M = -1, \quad \Omega = 1, \quad H = 2, \quad \lambda = 1, \quad E = 1, \quad K = 1.8$, and $\beta = -2$.

4.2. Advantages of the GA method

The GA method has a number of noteworthy methodological strengths. The main benefit derives from the fact that it can lead to closed-form analytical solutions, including trigonometric, exponential, and solitonic structures, which allow for a more transparent understanding of the underlying physical dynamics compared with purely numerical approximations [41]. Moreover, the technique is still reasonably manageable to implement, as the balancing procedure and subsequent algebraic manipulations tend to be less complex than those that have to be performed with many other analytical techniques. An additional salient feature of the GA approach is the flexibility of the approach, enabling the derivation of multiple classes of solitary–wave solutions in a single systematic way. The presence of explicit exact expressions further increases its usefulness for later qualitative analyses, where a more convenient study of its dynamical properties, such as the stability behavior and characteristics of bifurcations, which are often very difficult to identify through numerical simulations alone, is possible.

4.3. Limitations of GA method

Although the GA method has shown some success in various circumstances, it is not possible to apply it in a generalizable sense to all classes of nonlinear PDEs. Its successful deployment critically relies on the existence of a good balance between the terms with the highest order of derivatives and the nonlinear components inherent to the model. In the absence of such a balance, the method may not provide solutions that are both mathematically valid and physically meaningful. The difficulties encountered above are most acute in equations with highly irregular mathematical structure, strong nonlocal interactions, or discontinuous behavior. Moreover, problems that involve fractional order derivatives, stochastic influences, or piecewise nonlinear terms usually go beyond

the practical scope of the GA approach. For the more complex models, alternative analytical and computational strategies, including the homotopy analysis method, the variational iteration method, and direct numerical methods, often provide a more appropriate analysis strategy for reaching an accurate and relevant solution.

5. Phase portrait

Phase portrait analysis [37], and analyses of chaos make up a basic framework for understanding qualitative behavior in nonlinear systems. Recent studies have defined complex architectures of dynamical structures, bifurcations, and chaotic attractors in the context of nonlinear differential equations and the corresponding dynamical models. Of special relevance to this work, recent work on phase portraits and chaotic dynamics has made use of sophisticated analytical and numerical approaches applied to complex data–sets, and thereby discovered rich phenomena intrinsic in the nonlinear flow. This approach allows for very accurate transitions between periodic and chaotic flow regimes. Researchers interested in these developments include some quite recent contributions [38,39]. These advances have emphasized the essential part played by phase space analysis and by chaos theory in the development of our understanding of the complex dynamics of nonlinear systems.

In this section, we derive the system of equations below by applying the Galilean transformation to the ordinary differential equation in Eq (3.9):

$$\begin{cases} \frac{d\chi}{d\xi} &= \mathcal{P}, \\ \frac{d\mathcal{P}}{d\xi} &= -\Delta_a\mathcal{P} + \Delta_b\mathcal{R} - \Delta_c\mathcal{R}^3, \end{cases} \tag{5.1}$$

where $\Delta_a = \frac{(E^2+2F)\beta-2\omega}{2E^2\beta^2}$, $\Delta_b = \frac{G}{2E^2\beta^2}$, and $\Delta_c = \frac{H}{2E^2\beta^2}$. The first integral of the system Eq (5.1) is given by

$$\mathcal{K}_1(\mathcal{P},\Re) = \frac{(1+\Delta_a)}{2}\mathcal{P}^2 - \frac{1}{2}\Delta_b\Re^2 + \frac{1}{4}\Delta_c\Re^4. \tag{5.2}$$

To find the equilibrium points of the dynamical system (5.1), we solve the following system:

$$\begin{cases} \mathcal{P} = 0, \\ -\Delta_a\mathcal{P} + \Delta_b\mathcal{R} - \Delta_c\mathcal{R}^3 = 0. \end{cases} \tag{5.3}$$

The equilibrium points of the dynamical system (5.1) are given by

$$\mathcal{A}_0 = (0,0), \quad \mathcal{A}_1 = \left(\sqrt{\frac{\Delta_b}{\Delta_c}}, 0\right), \quad \mathcal{A}_2 = \left(-\sqrt{\frac{\Delta_b}{\Delta_c}}, 0\right).$$

At the equilibrium point (χ_0, ϕ_0), the Jacobian determinant is

$$\begin{aligned} \mathcal{K}_1(\mathcal{P},\Re) &= \begin{vmatrix} 0 & 1 \\ \Delta_b - 3\Delta_c\mathcal{R}^2 & \Delta_a \end{vmatrix} \\ &= -\Delta_b + 3\Delta_c\mathcal{R}^2. \end{aligned}$$

As suggested by the bifurcation theory of planar dynamical systems, we derive the following theorem.
Theorem 4. As a consequence, point $\mathcal{A}_0$ represents the saddle point if $\mathcal{K}_1(\mathcal{P},\Re) < 0$, indicates central

behavior if $\mathcal{K}_1(\mathcal{P}, \Re) > 0$, and $\mathcal{A}_0$ shows cusp behavior if $\mathcal{K}_1(\mathcal{P}, \Re) = 0$. Similarly, point $\mathcal{A}_1$ represents the saddle point if $\mathcal{K}_1(\mathcal{P}, \Re) < 0$, indicates central behavior if $\mathcal{K}_1(\mathcal{P}, \Re) > 0$, and $\mathcal{A}_1$ shows cusp behavior if $\mathcal{K}_1(\mathcal{P}, \Re) = 0$.

Moreover, point $\mathcal{A}_2$ represents the saddle point if $\mathcal{K}_1(\mathcal{P}, \Re) < 0$, indicates central behavior if $\mathcal{K}_1(\mathcal{P}, \Re) > 0$, and $\mathcal{A}_2$ shows cusp behavior if $\mathcal{K}_1(\mathcal{P}, \Re) = 0$.

Family 1. When $\Delta_b > 0$ and $\Delta_c > 0$, the system described by Eq (5.1) has three equilibrium points: $A_1 = (\sqrt{\frac{\Delta_b}{\Delta_c}}, 0)$, $A_2 = (-\sqrt{\frac{\Delta_b}{\Delta_c}}, 0)$, and $A_3 = (0, 0)$. By choosing suitable values of Δ_b=0.5 and Δ_c=0.2. We know that $\mathcal{K}_1(A_1) > 0$, indicating that A_1 is a central point, while $\mathcal{K}_1(A_2) > 0$, indicating that A_2 is also a central point, and similarly $\mathcal{K}_1(A_3) < 0$ so indicating that A_3 is a saddle point. The behavior is shown in Figure 3(a).

Family 2. When $\Delta_b < 0$ and $\Delta_c > 0$, the system described by Eq (5.1) has three equilibrium points: $A_1 = (\sqrt{\frac{\Delta_b}{\Delta_c}}, 0)$ and $A_2 = (-\sqrt{\frac{\Delta_b}{\Delta_c}}, 0)$, and $A_3 = (0, 0)$. By choosing the suitable values of Δ_b=–0.5 and Δ_c=–0.2. Here A_1 and A_2 are imaginary points. Therefore , we discuss the point $\mathcal{K}_1(A_3) > 0$ so indicating that A_3 is a central point. The behavior is shown in Figure 4(a).

Family 3. When $\Delta_b > 0$ and $\Delta_c < 0$, the system described by Eq (5.1) has three equilibrium points: $A_1 = (\sqrt{\frac{\Delta_b}{\Delta_c}}, 0)$ and $A_2 = (-\sqrt{\frac{\Delta_b}{\Delta_c}}, 0)$, and $A_3 = (0, 0)$. By choosing the suitable values of Δ_b=–0.5 and Δ_c=–0.2. Here A_1 and A_2 are imaginary point point. Therefore , we discuss the point $\mathcal{K}_1(A_3) > 0$ so indicating that A_3 is a saddle point. The behavior is shown in Figure 4(b).

Family 4. When $\Delta_b < 0$ and $\Delta_c < 0$, the system described by Eq (5.1) has three equilibrium points: $A_1 = (\sqrt{\frac{\Delta_b}{\Delta_c}}, 0)$, $A_2 = (-\sqrt{\frac{\Delta_b}{\Delta_c}}, 0)$, and $A_3 = (0, 0)$. By choosing suitable values of Δ_b=–0.5 and Δ_c=–0.2. We know that $\mathcal{K}_1(A_1) < 0$, indicating that A_1 is a saddle point, while $\mathcal{K}_1(A_2) < 0$, indicating that A_2 is also a saddle point; similarly, $\mathcal{K}_1(A_3) > 0$, thus indicating that A_3 is a center point. The behavior is shown in Figure 3(b).

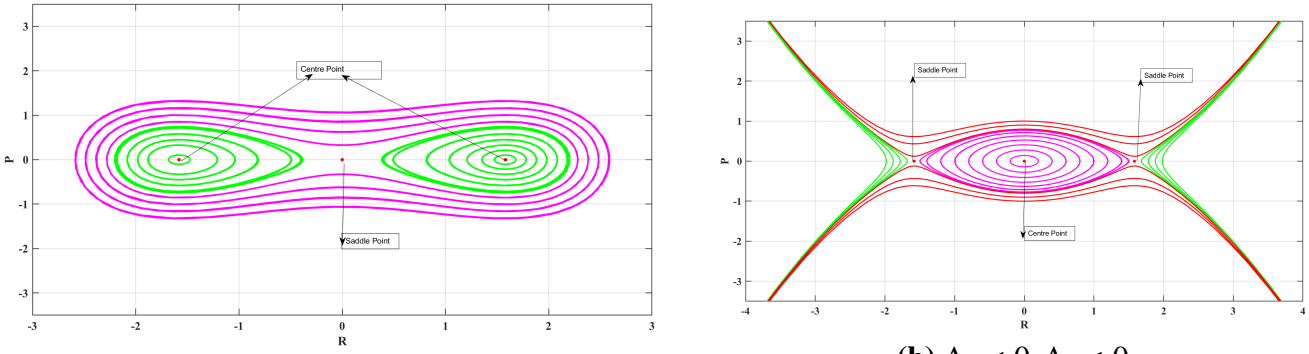

(a) $\Delta_b > 0, \Delta_c > 0$ **(b)** $\Delta_b < 0, \Delta_c < 0$

Figure 3. Phase trajectories of the dynamical system (5.1) when (a) $\Delta_b > 0, \Delta_c > 0$ and (b) $\Delta_b < 0, \Delta_c < 0$.

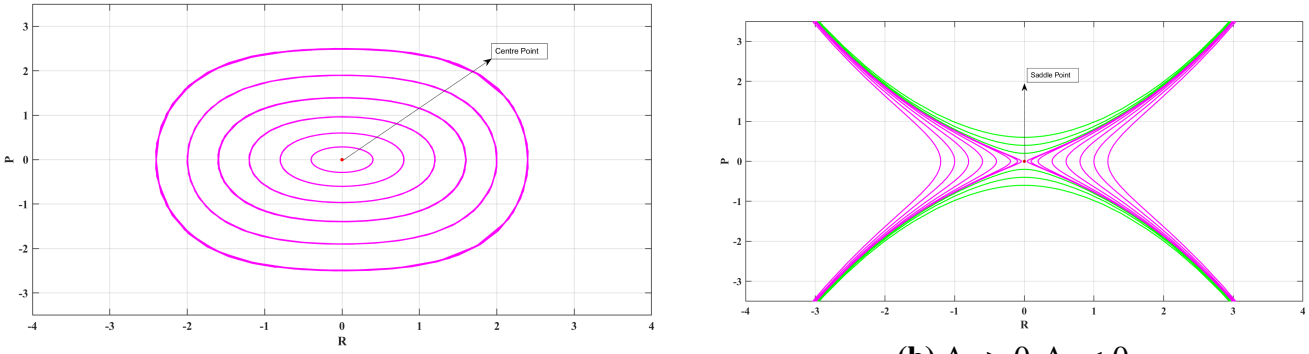

(a) $\Delta_b < 0, \Delta_c > 0$ **(b)** $\Delta_b > 0, \Delta_c < 0$

Figure 4. Phase trajectories of the dynamical system (5.1) when (a) $\Delta_b < 0, \Delta_c > 0$ and (b) $\Delta_b > 0, \Delta_c < 0$.

Phase portrait analysis is a very important tool for understanding the qualitative dynamics of nonlinear systems. Within this study, phase portraits are used to describe the trajectories of the reduced dynamical system on the phase plane, and the stability characteristics of equilibrium points are scrutinized. This analytical approach helps to expose the underlying solution's structure and provides a substantive insight into the dynamical behavior associated with the derived soliton solutions. Furthermore, the phase portraits support the results of the analysis and explain the transitions between different dynamical regimes of the system.

6. Chaotic behavior with perturbation term

To analyze the chaotic behavior [42] induced by periodic disturbances in Eq (5.1), we incorporate a disturbance factor, $\alpha cos(\beta\xi)$ [43], where α denotes the amplitude and β represents the frequency. The planar dynamical system can then be modeled using the following set of equations:

$$\begin{cases} \frac{d\mathcal{R}}{d\xi} &= \mathcal{P}, \\ \frac{d\mathcal{P}}{d\xi} &= -\Delta_a\mathcal{P} + \Delta_b\mathcal{R} - \Delta_c\mathcal{R}^3 + \alpha cos(\beta\xi). \end{cases} \tag{6.1}$$

The inclusion of a perturbation term $\alpha\, cos(\beta\xi)$ captures the external periodic influences on the financial system. Practically, this model accounts for cyclical factors such as seasonal effects, regulatory policies, and macroeconomic shocks, which recur over time. The parameter α measures the amplitude of these disturbances of the market, while the parameter β denotes the frequency of oscillation. Incorporation of this term has allowed us to study the influence of periodic exogenous shocks on the stability of the system and possible triggering of the transition from regular to chaotic dynamics, and thus capture the volatility clustering and irregular fluctuations that can be observed in real financial markets. Multiple analytical techniques were used to examine the chaotic properties of the system (6.1), with the aim of delimiting the dynamical characteristics of the system under various arbitrary values of the physical parameters. Temporal analysis is helpful for getting a complete picture of the dynamical evolution, stability, and periodicity of the considered system. The return map explains recurrent behavior and possible chaotic behavior by depicting successive points in the phase space. The two-dimensional (2D) phase portraits for Healthcare Solutions identify the trajectories of P and Q graphically and consequently reveal the equilibrium points, limit cycles, and attractors. Collectively,

these methodologies add to the detection of bifurcation diagrams, multistability, and the time series analysis of the initial conditions in the stipulated nonlinear framework. The effects of the parameter changes are investigated by means of 2D phase profiles and time series representations shown, e.g., in Figure 5 by the choice of the parametric values $\Delta_a = 0, \Delta_b = 0.02, \Delta_c = 0.3, \alpha = 0.8$, and $\beta = 0.9$ and the starting conditions (2.2, 1.7). In Figure 6, they are shown by selecting the parametric values $\Delta_a = 0, \Delta_b = 0.02, \Delta_c = 0.3, \alpha = 0.8$, and $\beta = 0.9$ and the initial conditions (2.2, 1.07). Figure 7 shows the results by selecting the parametric values $\Delta_a = 0, \Delta_b = 0.2, \Delta_c = 0.6, \alpha = 1.08$, and $\beta = 0.4$ and the initial conditions (2.2, 1.7). Under conditions of minimal intensity and frequency of the external forcing, the system (6.1) displays chaotic dynamics. This chaotic behavior is maintained by increasing the amplitude while generating unique structural behaviors. With the help of spectral analysis, different types of dynamics (periodic, quasi-periodic, and chaotic) can be distinguished from each other based on the frequency components. The Lyapunov exponent measures the sensitivity to the initial conditions and agrees with chaotic behavior, providing a positive value. Bifurcation diagrams reveal parameter-dependent transitions, which include the phenomena of period-doubling and the threshold for chaos.

Ultimately, however, the chaotic attractor provides a pictorial representation of the strange attractors, representing the essence of both deterministic chaos and the inbuilt unpredictability of the underlying system. The Lyapunov exponent defines whether or not there is chaos; a positive value indicates chaotic dynamics, while a negative value indicates a convergence. Figure 10(b) illustrates this behavior over time, showing the chaotic behavior as the Lyapunov exponent value. In Figure 10(b), we observe that the chaotic pattern of the stated model is evident due to the presence of a positive Lyapunov exponent. A chaotic attractor is described as shown in Figure 10(a) in the domain of [0.5,0,0.5]. We also plot the bifurcation diagram, which exhibits periodic behavior in the domain of [1,0,1] as shown in Figure 10(d).

In this part, we explore the phenomenon of multistability in a system incorporating a perturbed term from Eq (6.1). Multistability refers to the coexistence of multiple, potentially numerous, solutions within a given range of physical variables and distinct initial conditions in a dynamical system. Figure 8 illustrates phase portraits in red and blue for $\Delta_b = 0.02, \Delta_c = 0.3, \alpha = 0.8$, and $\beta = 0.9$, considering the initial conditions (2.2, 1.7) and (2, 1.5). Similarly, Figure 9 depicts phase portraits with the same color scheme for the parameter values $\Delta_b = 0.2, \Delta_c = 0.6, \alpha = 1.08$, and $\beta = 0.4$, but with different initial conditions, (2.5, 1.7) and (2.1, 1.7). Under these conditions, the system exhibits chaotic periodic behavior. Furthermore, we extend our investigation into the multistability of the nonlinear dynamical system.

Bifurcation and chaos analysis offer a theoretical framework to explain the transition across stable, periodic, and chaotic states when the value of some parameter is slightly changed. Within a financial realm, this framework emulates how the market's sensitivity to certain variables, like volatility and interest rates, can make the system sensitive to small perturbations in variables and cause flawed or erratic dynamics in price. The initial conditions are used for didactic purposes instead of empirical conditions and hence display dynamical patterns for plausible parameter combinations [45].

For enrichment of the analytical framework, the paper distinguishes periodic, quasi-periodic, and chaotic dynamics by using a few methodological approaches. In the case of the periodic regime, the time-series plot contains regular oscillations, although the corresponding chaotic portraits give closed orbits. Within the quasi-periodic regime, the phase portraits have toroidal-like trajectories, and the power-spectral density (PSD) has multiple incommensurate peaks, indicating oscillations with non-

integer frequency ratios. These diagnostic indicators are further supported by the Lyapunov exponent, return map, and bifurcation diagram. Collectively, these results show that the system is alternating across periodic, quasi-periodic, and chaotic states as the parameters change. This exhaustive analysis confirms that the model shows chaotic behaviors under perturbation and captures the intermediate dynamics that are seen to occur in financial systems exposed to cyclical shocks and instabilities.

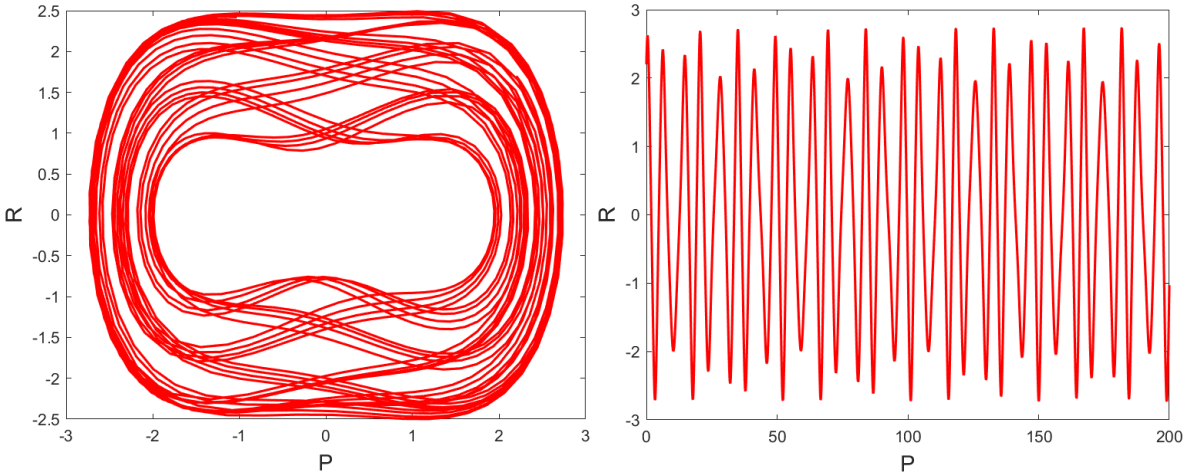

(a) 3D surface **(b)** 2D surface

Figure 5. Chaotic behavior of the dynamical system (6.1) by selecting the parametric values $\Delta_a = 0, \Delta_b = 0.02, \Delta_c = 0.3, \alpha = 0.8$, and $\beta = 0.9$ and the initial conditions (2.2, 1.7).

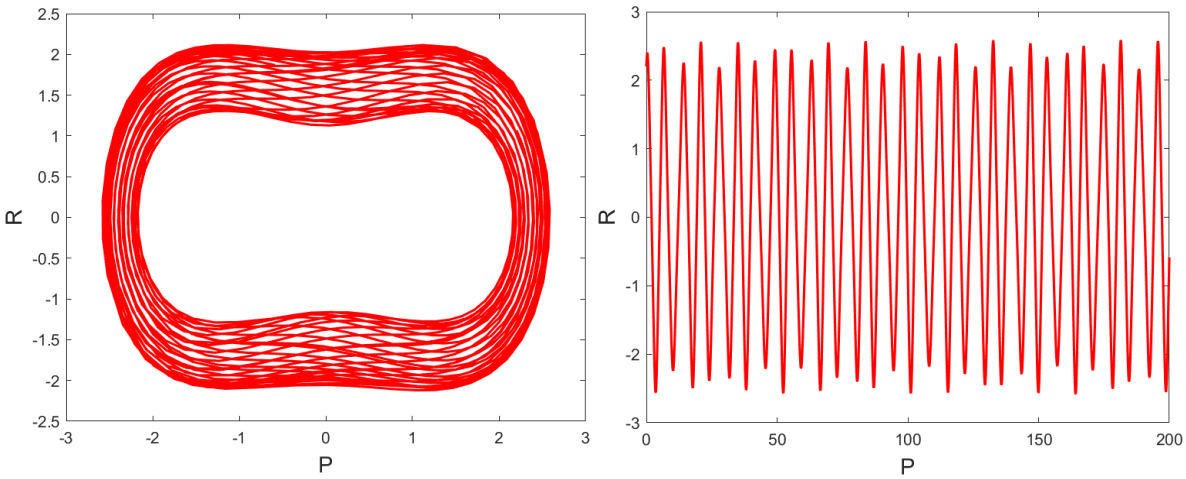

(a) 3D surface **(b)** 2D surface

Figure 6. Chaotic behavior of the dynamical system (6.1) by selecting the parametric values $\Delta_a = 0, \Delta_b = 0.02, \Delta_c = 0.3, \alpha = 0.8$, and $\beta = 0.9$ and the initial conditions (2.2, 1.07).

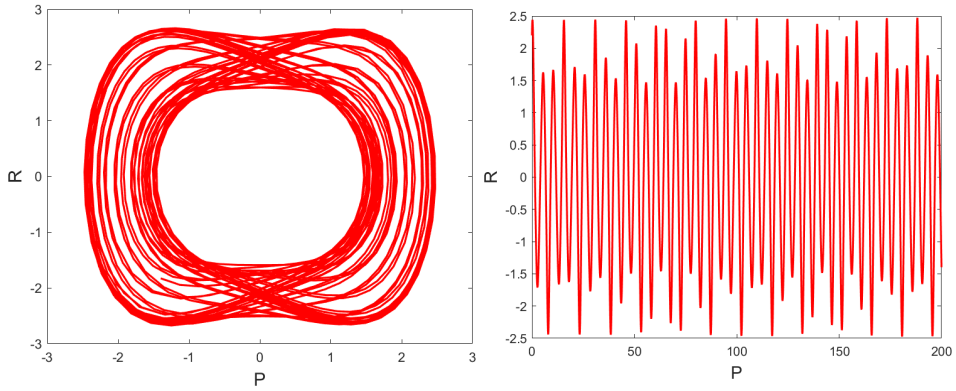

(a) 3D surface **(b)** 2D surface

Figure 7. Chaotic behavior of the dynamical system (6.1) by selecting the parametric values $\Delta_a = 0, \Delta_b = 0.2, \Delta_c = 0.6, \alpha = 1.08$, and $\beta = 0.4$ and the initial conditions (2.2, 1.7).

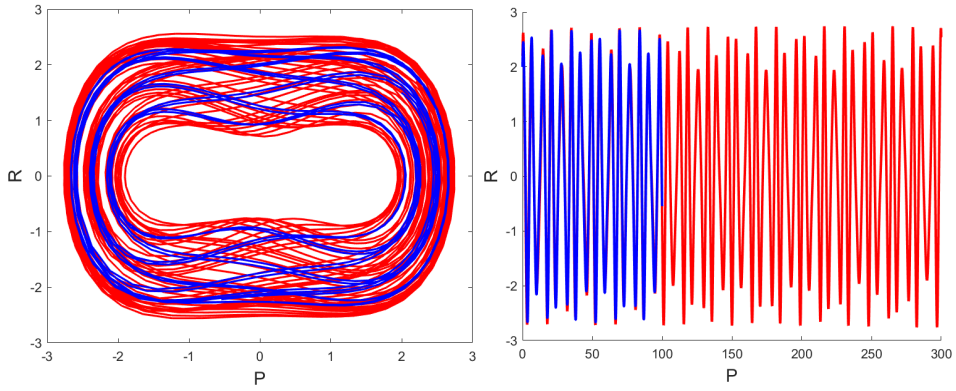

(a) 3D surface **(b)** 2D surface

Figure 8. Multistability analysis of the system (6.1) by using the parameters $\Delta_b = 0.02, \Delta_c = 0.3, \alpha = 0.8$, and $\beta = 0.9$, considering the initial conditions (2.2, 1.7) and (2, 1.5).

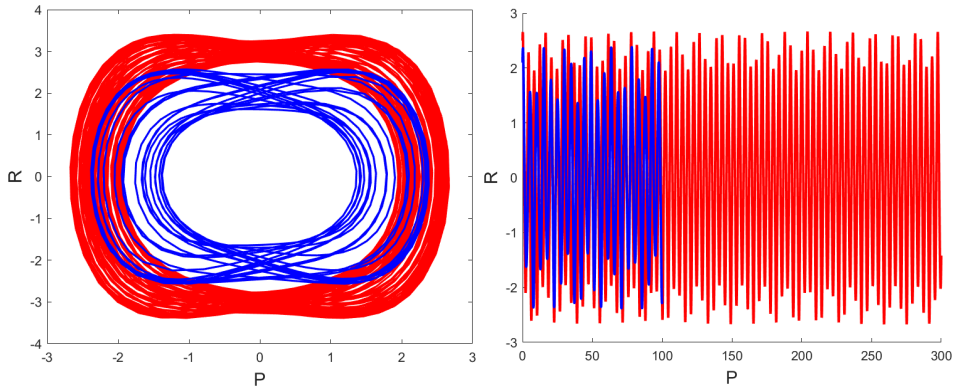

(a) 3D surface **(b)** 2D surface

Figure 9. Multistability analysis of the system (6.1) by using the parameters $\Delta_b = 0.2, \Delta_c = 0.6, \alpha = 1.08$, and $\beta = 0.4$, but with different initial conditions, (2.5, 1.7) and (2.1,1.7).

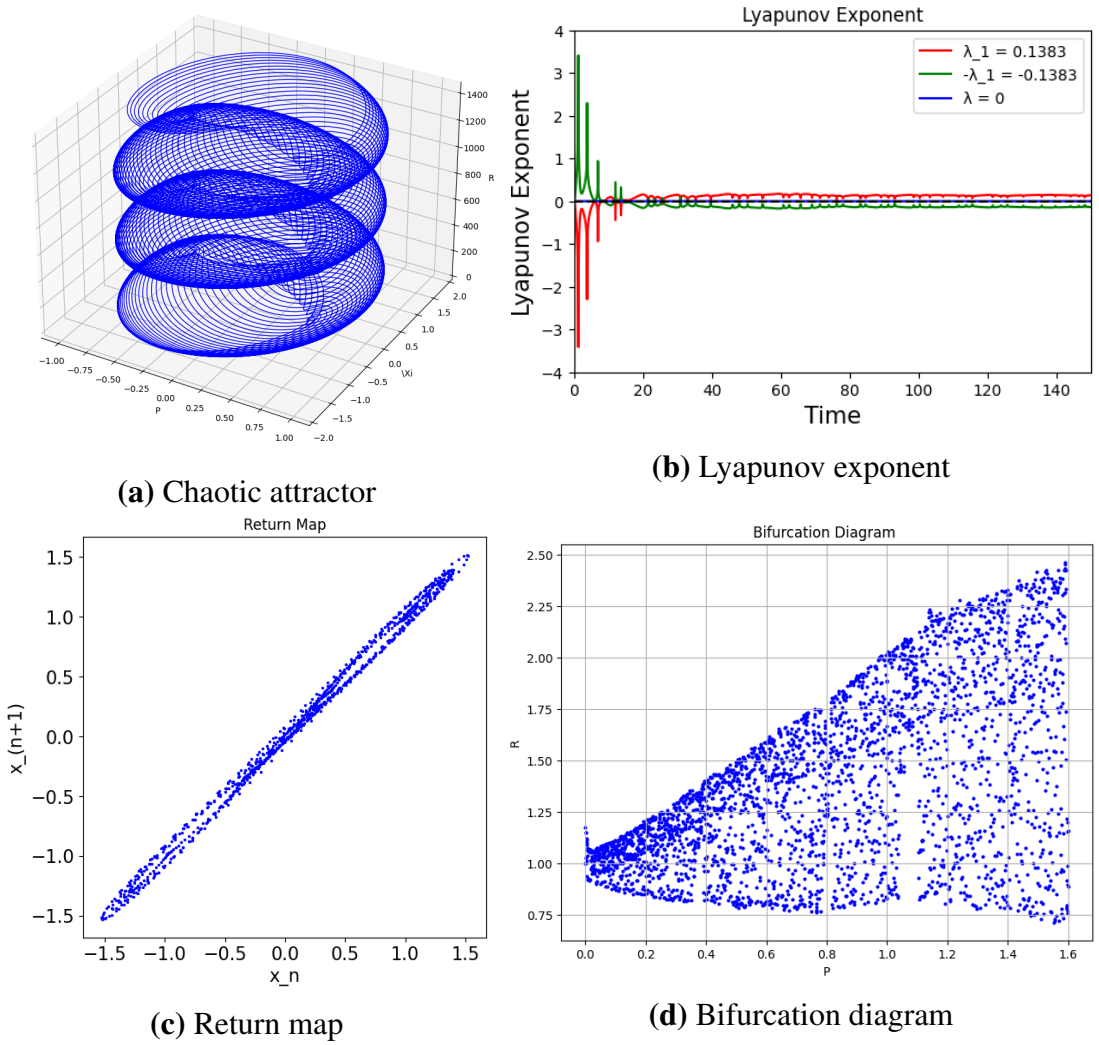

(a) Chaotic attractor

(b) Lyapunov exponent

(c) Return map

(d) Bifurcation diagram

Figure 10. Detection of chaos using different diagnostic tools: (a) Chaotic attractor, (b) Lyapunov exponent, (c) return map, and (d) bifurcation diagram.

7. Results and discussions

In this section, we present analytical and numerical findings driven by the generalized BSE, obtained through the GA method, using Lie symmetry analysis and nonlinear dynamical techniques. The focus is on both deriving solutions and clarifying their physical and financial significance in the stock market.

Solitary wave [44] solutions derived through the GA method include bright and dark solitons. From a financial perspective, these solutions represent localized deviations in option prices. A bright soliton corresponds to a sharp, localized increase in the option price, often representing a sudden upward shift in value due to market shocks. Conversely, a dark soliton signifies a localized dip in the option price linked to a short-term correction or temporary market slowdowns. This interpretation connects the soliton structures with financial market dynamics.

Bifurcation analysis illustrates that small parameter changes can drive transitions from stability to oscillation or chaos. This aligns with the financial market, where volatility, interest rates, or liquidity

fluctuations cause instability. The perturbation term $\alpha\, cos(\beta\xi)$ models the effect of cyclic shocks, which can produce periodic, quasi-periodic, or chaotic behavior. Sensitivity to the initial conditions reveals multistability, reflecting how markets under similar conditions may evolve differently depending on sentiment and starting positions.

Figure 1 illustrates the dark soliton solution of the Eq (4.8) with the parameters $G = 4, M = 1, \Omega = 1, H = 2, \lambda = -1, E = 1$, and $K = 1.8$. The three-dimensional (3D) surface and the 2D projection have a localized depression in the amplitude profile of the option value function. This indicates a temporary downward variation of the option price in comparison with its background level. Economically, it can be taken to mean a short-term correction or a temporary fall in market sentiment, provoking a temporary drop in the option value until equilibrium is re-established. The smooth localized geometry of the dark soliton may lead one to suspect that nonlinear effects within the generalized Black–Scholes model can give rise to a stable localized reduction in price dynamics.

Figure 2 represents the bright soliton solution of Eq (4.11) with the parameters $G = 4, M = -1, \Omega = 1, H = 2, \lambda = 1, E = 1, K = 1.8$, and $\beta = -2$. The graphical function shows a localized peak that moves in the transformed variable x, which indicates a significant step in the option price above the baseline. Such a bright soliton profile may be construed as a sudden up-movement in the option value due to strong nonlinear interactions within the financial market, possibly triggered by sudden flutters in demand or external economic shocks. The persistence of the localized peak shows the balance between the nonlinear effects and dispersion in the generalized model, and hence makes the formation of stable wave-like structures in option-pricing dynamics possible.

Figure 3 is the phase diagram of the reduced dynamical system given by Eq (5.1). In the case of the situation when $\Delta_b > 0$ and $\Delta_c > 0$, the phase trajectories show the coexistence of center-type equilibrium points and saddle-type equilibrium points. The center points correspond to oscillatory trajectories that are bounded around the equilibrium (indicating stable periodic behavior). On the other hand, for $\Delta_b < 0$ and $\Delta_c < 0$ saddle equilibrium produces unstable trajectories that move away from the point of equilibrium. The co-existence of these structures indicates the presence of stable oscillations and unstable motions in this dynamically active system, depending on the initial conditions and values for the evaluated parameters. This behavior reflects the alternation between the stable fluctuations and unstable transitions in the dynamics of option prices in the financial markets.

Figure 4 shows an alternative phase portrait for the dynamical system (5.1) at different parameter configurations. When $\Delta_b < 0$ and $\Delta_c > 0$, the phase trajectories have primarily center-type equilibrium, which indicates the periodic and stable oscillatory motion of phase trajectories around the equilibrium points. Conversely, when $\Delta_b > 0$ and $\Delta_c < 0$, saddle-type equilibria are the most important and draw the system into unstable trajectories, as they move further and further away from equilibrium states. This variation is a good demonstration that tiny changes in the system's parameters can lead to significant changes in the qualitative dynamics of the model. In terms of money, such transitions may be indicated by changes from a stable state of the market or unstable regimes initiated by fluctuations in volatility or in reaction to external economic factors.

Figure 5 shows the chaotic behavior of the perturbed dynamical system given by Eq (6.1) for a parameter set $\Delta_a = 0, \Delta_b = 0.02, \Delta_c = 0.3, \alpha = 0.8$, and $\beta = 0.9$ with the initial conditions (2.2, 1.7). The 3D trajectory and its corresponding 2D projection display irregular (non-periodic) motion, which is a common characteristic of chaotic motion. The trajectory never repeats itself but settles into no simple periodical orifice, thus showing the existence of complex nonlinear relationships inside the

system. These disordered variations may be interpreted as irregular fluctuations in the price of an option generated by capricious outside factors or market shocks.

Figure 6 shows the chaos dynamics with the same parameter values as in Figure 5, but with the initial condition perturbed to (2.2, 1.07). The calculated trajectory is very different from that in Figure 5 (even with identical parameter values) and thus highlights the very high sensitivity to initial conditions that is the hallmark of a chaotic system. The graphical results show that infinitesimal disturbances at the moment of inception can lead to radically different dynamical evolutions. Within a financial context, this translates to a mechanism by which slightly different starting conditions on the markets or investor sentiments cause vastly different option price timescales.

The chaotic dynamics of the system are presented for the parameter configuration $\Delta_a = 0, \Delta_b = 0.2, \Delta_c = 0.6, \alpha = 1.08$, and $\beta = 0.4$ and the initial conditions (2.2, 1.7) in Figure 7. The resulting 3D trajectory is a complex, bounded structure recognized as a chaotic attractor, whereas the 2D projection highlights the irregularity in the system's motion in the phase space. In contrast with periodic motion, the trajectory never repeats itself but is confined within a finite region, which shows the chaotic behavior of determinism. In the context of financial modeling, such behavior may be irregular fluctuations in option prices caused by the nonlinear interactions and external periodic perturbations in the market environment.

Figure 8 zooms in on the phenomenon of multistability in the dynamical system, which is associated with the parameter values $\Delta_b = 0.02, \Delta_c = 0.3, \alpha = 0.8$, and $\beta = 0.9$. The two initial conditions are (2.2, 1.7) and (2,1.5). The subsequent trajectories have divergent trajectories towards different stable attractors, meaning that the system contains different, more stable states under the same parameter values. This behavior shows that long-term behavior in the system is strongly dependent upon the initial configuration. From a financial viewpoint, multistability means that markets with similar economic conditions can be driven towards different price patterns depending on how the market was initiated by the investors or initial market events.

The multistability is further highlighted in Figure 9 where the parameter values $\Delta_b = 0.2, \Delta_c = 0.6, \alpha = 1.08$, and $\beta = 0.4$ are chosen. Two initial conditions, (2.5, 1.7) and (2.1,17), give qualitatively different trajectories in phase space. Although the system's parameters are the same, the trajectories converge towards different attractors, confirming that there are several stable regimes. This phenomenon is a good example of how nonlinear financial models can model complex behaviors such as regime switching, in which the markets can switch between different states depending on the configuration and external influences at the beginning.

A complete diagnostic analysis of chaos in the dynamical system is provided in Figure 10. Figure 10(a) shows the chaotic attractor, which shows irregular motion that is bounded in phase space. Figure 10(b) shows the Lyapunov exponent, in which values above zero support the existence of chaos involving the exponential divergence of trajectories that are close to each other. Figure 10(c) shows the return map, which shows a non-repeating pattern typical for chaotic systems. Finally, Figure 10(d) shows the bifurcation diagram, showing the transitions from the periodic to the chaotic regime with the change of system parameters. Collectively, these diagnostic tools verify that the generalized Black–Scholes model can have complex nonlinear dynamics, hence providing a theoretical explanation of the irregular price fluctuation and clustering of volatility, as similarities are observed in the financial market.

The results show that the concepts of nonlinear dynamics and chaos provide a framework for

modeling irregular price fluctuations and volatility clustering in the option markets. This view supplements the traditional paradigm of the Black–Scholes type, which assumes a smooth course of prices and efficient functioning of the markets. However, the current investigation is rather theoretical in nature, as the chosen values of the parameters and initial conditions used are explanatory rather than empirically fitted to financial data. While this is a limitation in terms of direct empirical application, what is being highlighted is a novel way to weave nonlinear wave analysis, chaos theory, and multistability into financial models. Further research work related to the above could concentrate on calibration of the parameters against historical option price data, the calibration of the predictive power of the non–linear framework, and extension of the above mentioned results to a multi–asset environment or stochastic volatility models.

8. Comparison with previous literature

To put the methodological development into perspective, Table 2 compares the analytical, numerical, and hybrid approaches that have been used in solving the generalized BSE in the past. This overview outlines the respective features, benefits, limitations, and categories of solutions, thereby emphasizing the contribution of the present study to the literature.

The comparative summary given in Table 2 demonstrates that the proposed GA method gives improved analytical precision and wider applicability compared with the previous analytical and numerical methods. Consequently, this implies its usefulness for studying nonlinear and wave-structured solutions associated with financial and physical modeling.

Table 2. Comparison of analytical, numerical, and hybrid methods applied to the generalized BSE.

Method	Reference(s)	Features	Advantages	Limitations	Types of Solutions
Binomial / trinomial Tree	Cox et al. [11]; Hull [12]	Discrete-time lattice models	Simple and intuitive; widely used in finance	Approximate; less efficient for complex derivatives	—
Finite difference	Courtadon [13]; Brennan [14]	Numerical discretization of PDE	Flexible; handles boundary conditions	Only numerical; no explicit forms	—
Jump–diffusion	Merton [6]	PDE with jump processes	Captures sudden asset price jumps	Complex calibration; still linear	—
Fractional BSE	Ouafoudi [15]; Edeki [22]; Vijayan [23]	Fractional derivatives; memory effects	Captures heavy tails and long memory	Often approximate; requires transforms	—
Transform and series	Sobamowo [18]; Fadugba [17, 21]	Taylor or Laplace series expansions	Semi-analytical; improved accuracy	Convergence issues; limited generality	—
Neural networks	Santos [24]	Data-driven, machine learning approach	No explicit model required; adaptable	Requires training data; no analytical form	—
Chebyshev / polynomial	Afiatdoust [28]	Polynomial expansions into algebraic form	Reduces computational complexity	Accuracy depends on polynomial order	—
Conformable / fractional	Ait Brahim [29]; Morales-Bañuelos [31]; Vijayan [32]	Conformable fractional derivatives	Better empirical performance	More parameters; requires numerical support	—
GA	**Present work**	Symbolic balancing of the highest derivative with nonlinear terms	Provides exact analytical solitary wave solutions	Not applicable to irregular, fractional, or stochastic PDEs	Bright, dark, trigonometric, and exponential waves

9. Conclusions

In this study, a generalized nonlinear BSE was analyzed using analytical and dynamical methods. Initially, Lie symmetry analysis was used to identify infinitesimal generators and perform symmetry reductions, thereby reducing the PDE to an ODE. Based on these findings, the GA method was used to obtain a set of exact analytical solutions, including bright and dark soliton solutions and exponential-type solutions. These solutions provide insights into localized variations of option prices, which may occur as a consequence of the non–linear market effects. The dynamical properties of the reduced system were further analyzed using phase – portrait analysis, investigation of the bifurcations, and

chaos diagnostics. By adding a periodic perturbation term, the system was shown to go through transitions across periodic, quasi-periodic, and chaotic regimes. The detection of positive Lyapunov exponents, the appearance of strange attractors, and the finding of patterns of bifurcations are evidence of the existence of chaotic dynamics and multistability in the model. Overall, the findings demonstrate that nonlinear extensions of the BSE are able to capture complicated dynamic behaviors that are not contained in the classical model. The combination of Lie symmetry methods, exact analytical results, and chaos analysis provides a full framework for the study of nonlinear financial models. Prospective research directions may include calibration of the model's parameters to (empirical) market data and developing the methodology for multiple asset setups or for stochastic volatility models.

Author contributions

Khizar Farooq: Software, formal analysis, methodology, editing, writing–review; Ali. H. Tedjani: Investigation, formal analysis; Muhammad Amin S. Murad: review and investigation; Yakup Yildirim: Formal analysis, methodology, review; Taha Radwan: Investigation, validation, resources, funding acquisition. All authors have read and agreed to publish the manuscript.

Use of Generative-AI tools declaration

The authors declare that they have not used artificial intelligence (AI) tools in the creation of this article.

Acknowledgments

The researchers would like to thank the Deanship of Graduate Studies and Scientific Research at Qassim University for financial support (QU-APC-2026).

Conflict of interest

The authors declare no conflicts of interest to report regarding the present study.

References

1. F. Black, M. Scholes, The pricing of options and corporate liabilities, *J. Polit. Econ.*, **81** (1973), 637–654. Available from: https://www.jstor.org/stable/1831029.
2. T. Ahmad, H. X. Chen, A review on machine learning forecasting growth trends and their real-time applications in different energy systems, *Sustain. Cities Soc.*, **54** (2020), 102010. https://doi.org/10.1016/j.scs.2019.102010
3. J. Hadamard, Implied volatility in Black–Scholes model with GARCH volatility, *J. Math. Pure. Appl.*, **8** (1892), 101–186.
4. R. C. Merton, Theory of rational option pricing, *Bell J. Econ. Manag. Sci.*, **4** (1973), 141–183. https://doi.org/10.2307/3003143

5. S. L. Heston, A closed-form solution for options with stochastic volatility with applications to bond and currency options, *Rev. Financ. Stud.*, **6** (1993), 327–343. https://doi.org/10.1093/rfs/6.2.327
6. R. C. Merton, Option pricing when underlying stock returns are discontinuous, *J. Financ. Econ.*, **3** (1976), 125–144. https://doi.org/10.1016/0304-405X(76)90022-2
7. J. C. Hull, S. Basu, *Options, futures, and other derivatives*, Delhi: Pearson Education India, 2016.
8. B. Dupire, Pricing with a smile, *Risk*, **7** (1994), 18–20.
9. P. Wilmott, Derivatives: The theory and practice of financial engineering, 1998.
10. W. Gao, Y. Hu, The exact traveling wave solutions of a class of generalized Black–Scholes equation, *AIMS Math.*, **2** (2017), 385–399. https://doi.org/10.3934/Math.2017.3.385
11. J. C. Cox, S. A. Ross, M. Rubinstein, Option pricing: A simplified approach, *J. Financ. Econ.*, **7** (1979), 229–263. https://doi.org/10.1016/0304-405X(79)90015-1
12. J. Hull, A. White, The use of the control variate technique in option pricing, *J. Financ. Quant. Anal.*, **23** (1988), 237–251. https://doi.org/10.2307/2331064
13. G. Courtadon, A more accurate finite difference approximation for the valuation of options, *J. Financ. Quant. Anal.*, **17** (1982), 697–703. https://doi.org/10.2307/2330857
14. M. J. Brennan, E. S. Schwartz, Finite difference methods and jump processes arising in the pricing of contingent claims: A synthesis, *J. Financ. Quant. Anal.*, **13** (1978), 461–474. https://doi.org/10.2307/2330152
15. S. Bossu, P. Carr, A. Papanicolaou, A functional analysis approach to the static replication of European options, *Quant. Financ.*, **21** (2021), 637–655. https://doi.org/10.1080/14697688.2020.1810857
16. M. Ouafoudi, F. Gao, Exact solution of fractional Black–Scholes European option pricing equations, *Appl. Math.*, **9** (2018), 86.
17. S. E. Fadugba, A. A. Adeniji, M. C. Kekana, J. T. Okunlola, O. Faweya, Direct solution of Black–Scholes–Merton European put option model on dividend yield with modified-log payoff function, *Int. J. Anal. Appl.*, **20** (2022), 54. https://doi.org/10.28924/2291-8639-20-2022-54
18. G. M. Sobamowo, Analysis of Black–Scholes option pricing differential equations powered by log-payoff function using method of partial Taylor series expansion, *World Sci. News*, **172** (2022), 118–130.
19. G. Tour, N. Thakoor, D. Y. Tangman, Spectrally accurate option pricing under the time-fractional Black–Scholes model, *ANZIAM J.*, **63** (2021), 228–248. https://doi.org/10.1017/S1446181121000286
20. M. O. Durojaye, J. A. Kazeem, A semi-analytical solution of the Black–Scholes pricing model for European call option, *Direct Res. J. Eng. Inf. Technol.*, **7** (2020), 55–57.
21. S. E. Fadugba, O. H. Edogbanya, Comparative study of two semi-analytical methods for the solution of time-fractional Black–Scholes equation in a Caputo sense, *Trends Appl. Sci. Res.*, **15** (2020), 110–114.
22. S. O. Edeki, R. M. Jena, S. Chakraverty, D. Baleanu, Coupled transform method for time–space fractional Black–Scholes option pricing model, *Alex. Eng. J.*, **59** (2020), 3239–3246. https://doi.org/10.1016/j.aej.2020.08.031

23. C. Vijayan, R. Manimaran, Application of homotopy analysis Shehu transform method for fractional Black–Scholes equation, *IAENG Int. J. Appl. Math.*, **53** (2023), 1–9.
24. D. D. S. Santos, T. A. E. Ferreira, Neural network learning of Black–Scholes equation for option pricing, *Neural Comput. Appl.*, **37** (2025), 2357–2368. https://doi.org/10.1007/s00521-024-10761-7
25. E. Ngondiep, An efficient numerical approach for solving three-dimensional Black–Scholes equation with stochastic volatility, *Math. Method. Appl. Sci.*, **48** (2025), 4769–4789. https://doi.org/10.1002/mma.10576
26. V. Chandrasekaran, M. Rajendran, R. Nagarajan, Solving two-dimensional Black–Scholes equation by conformable Shehu homotopy analysis method, *Math. Model. Eng. Probl.*, **12** (2025), 629.
27. T. V. Zavyalova, G. A. Timofeeva, Study of the dynamics of abrupt changes in price in the generalized Black–Scholes model, *J. Math. Sci.*, **288** (2025), 87–91. https://doi.org/10.1007/s10958-025-07667-7
28. F. Afiatdoust, M. M. Hosseini, M. H. Heydari, Generalized shifted Chebyshev polynomials for time fractional Black–Scholes model, *Comput. Econ.*, 2025. https://doi.org/10.1007/s10614-025-10999-w
29. A. A. Brahim, K. Hilal, A. E. Hajaji, Pricing options in new generalized fractional Black–Scholes model, *Filomat*, **39** (2025), 407–422. https://doi.org/10.2298/FIL2502407B
30. N. Sukwong, W. Sawangtong, T. Sitthiwirattham, P. Sawangtong, Applying the generalized Laplace residual power series method to the time-fractional multi-asset Black–Scholes European option pricing model, *Contemp. Math.*, **6** (2025), 3809–3831. https://doi.org/10.37256/cm.6320257266
31. P. M. Bañuelos, S. E. R. Bojalil, L. A. Q. Téllez, G. F. Anaya, A general conformable Black–Scholes equation for option pricing, *Mathematics*, **13** (2025), 1576. https://doi.org/10.3390/math13101576
32. C. Vijayan, R. Manimaran, N. Racshitha, Fractional Black–Scholes equation described by the conformable fractional derivative with three different methods, *Int. J. Math. Oper. Res.*, 2025, 135–151. https://doi.org/10.1504/IJMOR.2025.145604
33. H. Hussain, E. Ejaz, R. A. Aljethi, K. Farooq, S. A. A. Shah, Lie symmetry analysis, rogue waves, and lump waves of nonlinear integral Jimbo–Miwa equation, *Symmetry*, **17** (2025), 1717. https://doi.org/10.3390/sym17101717
34. J. Yu, Y. Feng, Group classification of time fractional Black–Scholes equation with time-dependent coefficients, *Fract. Calc. Appl. Anal.*, **27** (2024), 2335–2358. https://doi.org/10.1007/s13540-024-00339-4
35. H. Zhang, Z. Wang, Optimal system, invariant solutions and conservation laws of the hyperbolic geometry flow with time-dependent dissipation, *J. Geom. Phys.*, **183** (2023), 104702. https://doi.org/10.1016/j.geomphys.2022.104702
36. M. A. S. Murad, F. S. Alshammari, M. S. Salih, K. Farooq, Optical soliton structures in the nonlinear conformable Schrödinger equation with quadratic–cubic nonlinearity, *Nonlinear Dynam.*, **113** (2025), 32669–32687. https://doi.org/10.1007/s11071-025-11775-z

37. Z. A. A. Saad, M. A. S. Murad, F. M. Omar, A. H. Tedjani, K. Farooq, Nonlocal effects and chaotic wave propagation in the cubic–quintic nonlinear Schrödinger model for optical beams, *Symmetry*, **17** (2025), 2129. https://doi.org/10.3390/sym17122129

38. Y. Zhang, C. Zhang, K. J. Wang, Qualitative analysis of the fractal complex Hirota-dynamical model for optical fiber communication: Variational principle, Hamiltonian and diverse soliton solutions, *Fractals*, 2026, 2650022. https://doi.org/10.1142/S0218348X26500222

39. Y. H. Liang, K. J. Wang, Bifurcation analysis, chaotic phenomena, variational principle, Hamiltonian, solitary and periodic wave solutions of the fractional Benjamin–Ono equation, *Fractals*, **33** (2025), 2550016. https://doi.org/10.1142/S0218348X25500161

40. K. Farooq, A. H. Tedjani, Z. Li, E. Hussain, Soliton dynamics of the nonlinear Kodama equation with M-truncated derivative via two innovative schemes: the generalized Arnous method and the Kudryashov method, *Fractal Fract.*, **9** (2025), 436. https://doi.org/10.3390/fractalfract9070436

41. K. Farooq, F. S. Alshammari, Z. Li, E. Hussain, Soliton dynamics and stability in the Boussinesq equation for shallow water applications, *Front. Phys.*, **13** (2025), 1637491. https://doi.org/10.3389/fphy.2025.1637491

42. K. Farooq, R. A. Aljethi, E. Hussain, M. A. S. Murad, Chaos, Lyapunov exponent, and sensitivity demonstration of the coupled nonlinear integrable model with soliton solutions, *AIMS Math.*, **10** (2025), 22929–22957. https://doi.org/10.3934/math.20251019

43. K. J. Wang, H. W. Zhu, S. Li, F. Shi, G. Li, X. L. Liu, Bifurcation analysis, chaotic behaviors, variational principle, Hamiltonian and diverse optical solitons of the fractional complex Ginzburg–Landau model, *Int. J. Theor. Phys.*, **64** (2025), 134. https://doi.org/10.1007/s10773-025-05977-9

44. K. Farooq, E. Hussain, U. Younas, H. Mukalazi, T. M. Khalaf, A. Mutlib, et al., Exploring the wave's structures to the nonlinear coupled system arising in surface geometry, *Sci. Rep.*, **15** (2025), 11624. https://doi.org/10.1038/s41598-024-84657-w

45. E. Hussain, R. A. Aljethi, K. Farooq, U. Younas, Optical multi-peakon dynamics in the fractional cubic–quintic nonlinear pulse propagation model using a novel integral approach, *Fractal Fract.*, **9** (2025), 631. https://doi.org/10.3390/fractalfract9100631

AIMS Press